

PAWEŁ BOROŃ, JOANNA DULIŃSKA*

SEISMIC PERFORMANCE OF A REINFORCED CONCRETE BRIDGE UNDER A SEQUENCE OF SEISMIC SHOCKS USING THE CONCRETE DAMAGE PLASTICITY MODEL

ODPOWIEDŹ DYNAMICZNA MOSTU ŻELBETOWEGO NA SEKWENCJĘ WSTRZĄSÓW SEJSMICZNYCH Z ZASTOSOWANIEM MODELU BETONU PLASTYCZNEGO ZE ZNISZCZENIEM

Abstract

This paper investigates the dynamic performance of a concrete bridge under a sequence of earthquakes. The PGA of the mainshock and the aftershock were comparable. The concrete damage plasticity model of material was assumed to represent the plastic behaviour of the bridge. Firstly, the mainshock was applied to the bridge, then the aftershock was imposed on the structure which had already been weakened by the first shock. The analysis of plastic and damage measures revealed that the aftershock had a considerable effect upon the structure in terms of enlarging zones affected by irreversible strains or additional damage evolution.

Keywords: seismic sequence, reinforced concrete bridge, concrete damage plasticity model

Streszczenie

W artykule przedstawiono analizę odpowiedzi dynamicznej mostu żelbetowego na sekwencję wstrząsów sejsmicznych. Wartości PGA dla wstrząsu głównego oraz wtórnego były porównywalne. W celu przedstawienia plastycznej pracy konstrukcji zastosowano model betonu plastycznego ze zniszczeniem. Analiza stref plastycznych oraz uszkodzeń elementów wykazała znaczący wpływ obu wstrząsów na konstrukcję. Wstrząs wtórny, działający na konstrukcję wcześniej uszkodzoną przez wstrząs główny, wywołuje zwiększenie strefy odkształceń plastycznych, rozwój zarysowań oraz degradację sztywności.

Słowa kluczowe: wstrząs wtórny, most żelbetowy, model betonu plastyczny ze zniszczeniem

* M.Sc. Eng. Paweł Boroń, Prof. D.Sc. Ph.D. Eng. Joanna Dulińska, Institute of Structural Mechanics, Cracow University of Technology.

1. Introduction

Within a short period of time, large seismic events are usually followed by several aftershocks. Since aftershocks affect structures that have already been weakened during a mainshock, they can play a crucial role in the dynamic behaviour of a structure in terms of irreversible plastic strains and accumulated damage. Structures may go plastic or even collapse during aftershocks since they have already become degraded and cracked during main shocks.

Over the last decade, the dynamic response of structures under replicated seismic shocks has been extensively studied. Concrete structures in particular may suffer severe damage when exposed to a sequence of earthquakes [5, 6, 11]. Representative examples of damage to structures observed under multiple earthquakes can be found in contemporary studies [1, 2].

In the paper, the dynamic performance of a reinforced concrete bridge subjected to a mainshock-aftershock seismic sequence is investigated. In order to compare damages under repeated shocks and assess the impact of both events on the bridge, the concrete damage plasticity model, which describes multi-hardening plasticity and damage (cracking), was implemented. Only advanced constitutive models of concrete, that include damage and failure phenomena, may demonstrate inelastic behaviour and progressive damage of the concrete bridge under repetitive shocks.

2. Basic parameters of the structure

In this study, an existing reinforced concrete bridge was analysed as a structure subjected to a sequence of seismic shocks. The total length of the three-span road bridge was 84 m. The length of the middle span was 29 m and the length of the outer spans was 27.5 m (Fig. 1).

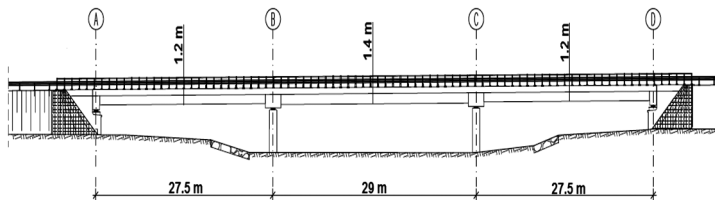


Fig. 1. The three-span reinforced concrete bridge – side view

The bridge was built as a pre-stressed concrete beam-slab structure. Every span consisted of eleven prefabricated reinforced T-shape beams (Fig. 2). T24 and T27 beams were used in the outer and the middle spans, respectively. These types of beam differed from each other with respect to their dimensions. The dimensions of the T27 beam were as follows: height – 110 cm, width of lower part – 27 cm, width of top part – 84 cm. The dimensions of the T24 beam were slightly different: height – 100 cm, width of bottom part – 24 cm, width of top – part 84 cm. The beams were made of B50 (C40/45) concrete. Each beam was equipped with twenty-four pre-stressing tendons with a diameter of 15.5 mm to produce the compressive stress that balanced the tensile stress that the girders would otherwise experience.

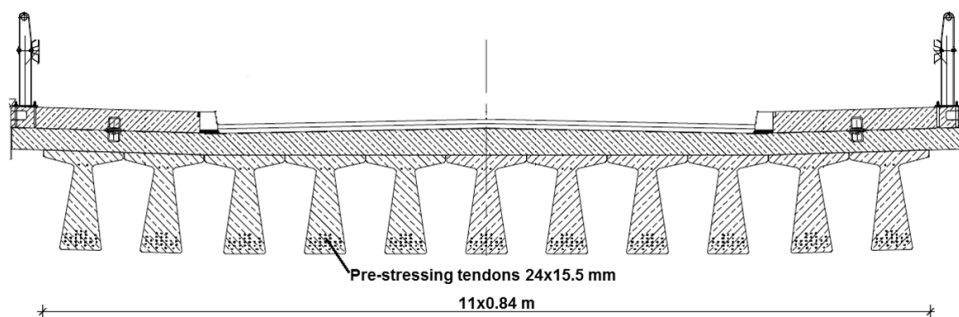


Fig. 2. The cross-section of the bridge superstructure

The bridge deck was built as a slab monolithically connected with the beams. The slab thickness varied from 20 cm at the thinnest point to 30 cm at the thickest point. The bridge superstructure was supported on pillars and abutments by stiff bearings. There were four bearings located on every support.

3. The numerical model of the bridge

In order to carry out the dynamic analysis of the bridge, a numerical model of the structure was created using the ABAQUS software [12]. In the model, all structural elements (i.e. beams, slabs, bearings, pillars and abutments) were taken into account. The geometry and dimensions of the elements were taken from the technical description of the object.

In the model, a link between the top surface of the beam and the slab was provided by a 'TIE' constraint that makes the translational and rotational degrees of freedom equal for a pair of surfaces [12]. The pre-stressing tendons of the beams and the reinforcement of the bridge slab were also taken into consideration in the model since the ABAQUS software allows for the insertion of rebar layers into concrete structures as 'fuzzy layers' [5].

It was assumed that the bridge is located on stiff subsoil; therefore, the soil-structure interaction was not considered. The fixed boundary conditions were imposed on pillars and abutments that reflected the high rigidity of the bridge subsoil.

Two kinds of finite elements, provided by the ABAQUS software, were used in the numerical model – solid elements C3D8R and continuum shell elements CS8R (8 nodes with 3 degree of freedom in both cases). Solid elements were used to model the beams, the pillars and the abutments, whereas the thin slab was discretised with continuum shell elements. Such a manner of discretisation allowed a reduction of the number of degree of freedom in the entire model and the accelerations of calculations. To improve the efficiency of calculations, the FE mesh was densified only in areas where stress concentration was predicted (i.e. in the middle of each span and at the ends of each beam). In total, the mesh consisted of around 150.000 solid and 23.000 shell elements. Further densification of the mesh did not introduce noticeable changes to the results.

The numerical model of the bridge is shown in Fig. 3. The meshing of the beams is shown in Fig. 4. The beam located in the central span of the bridge with the FE mesh densified in the middle of span and at the end is presented in Fig. 4a; the details of the FE mesh of the beam end are displayed in Fig. 4b.

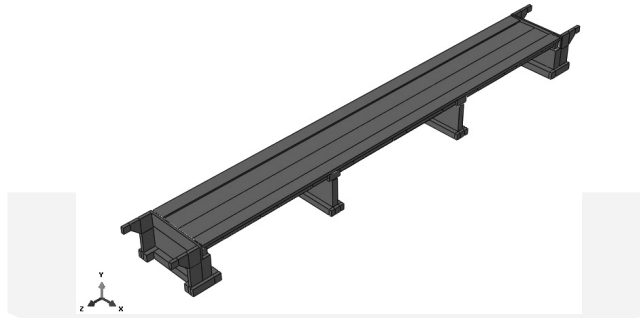


Fig. 3. The numerical model of the bridge

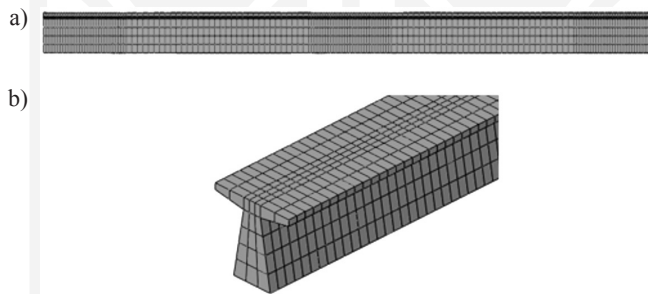


Fig. 4. (a) FE mesh densified in the middle of the span and at the end of the beam located in the central span; (b) details of the FE mesh used for the analysis of the pre-stressed concrete beam

4. Parameters of the concrete damage plasticity material model

To represent the elastic-plastic behaviour of the concrete bridge under a sequence of seismic shocks, the concrete damage plasticity model (CDP) was assumed as a constitutive model of the concrete material [8, 10]. The CDP model, implemented in the ABAQUS software, allows the description of all phenomena typical of the concrete material that occur during cyclic loading [3, 4, 9]. The CDP model uses concepts of the combination of non-associated multi-hardening plasticity and scalar damaged elasticity to represent the inelastic behaviour of concrete and to describe the irreversible damage that occurs during the fracturing process.

Different material parameters for tension and compression were defined in the model that allowed precise imitation of the realistic behaviour of the concrete material in a complex state of stress. Stress-strain dependence in tension and in compression for B50 concrete is shown in Fig. 5a and 5b, respectively [7].

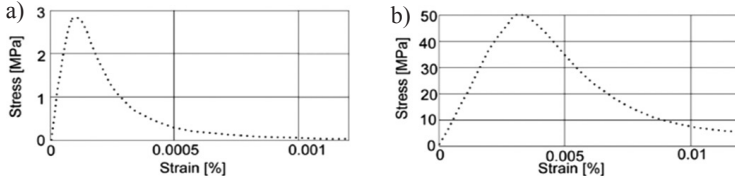


Fig. 5. Dependence σ – ε for B50 concrete in: (a) tensile test, (b) compression test [7]

Except typical engineering measure, like strain, logarithmic strain or equivalent plastic strain could be analysed in this model of concrete material. In large deformation analysis, logarithmic strain (LE) allows the description of strain more precisely than engineering measures. Expressing strain in a logarithmic form allows the comparison of the current element length directly with the initial element length. This strain could be described by equation (1):

$$\varepsilon = \ln \frac{l_0 + \Delta l}{l_0} = \ln \frac{l_1}{l_0} \quad (1)$$

where:

- l_0 – initial length,
- l_1 – current length,
- Δl – increase in length.

In the CDP model, the effect of material damage is taken into consideration. The yield surface is controlled by two hardening variables representing equivalent plastic strains: $\tilde{\varepsilon}_t^{pl}$ and $\tilde{\varepsilon}_c^{pl}$, linked to failure mechanisms under tension and compression loading, respectively. To describe the damage process of the concrete material stiffness degradation, scalar value d , tensile damage variable d_t , compressive damage variable d_c are implemented (SDEG, DAMAGET and DAMAGEC, respectively).

Tensile and compressive stiffness degradation parameters depend on the level of equivalent plastic strain $\tilde{\varepsilon}^p$:

$$d_c = d_c(\tilde{\varepsilon}_c^{pl}) \quad (2.1)$$

$$d_t = d_t(\tilde{\varepsilon}_t^{pl}) \quad (2.2)$$

where:

- $\tilde{\varepsilon}_c^{pl}$ – compressive equivalent plastic strain,
- $\tilde{\varepsilon}_t^{pl}$ – tension equivalent plastic strain.

Equivalent plastic strain $\tilde{\varepsilon}^{pl}$ (marked in the ABAQUS as PEEQ – for compression, PEEQT – for tension) describes the total plastic strain level in elements. This parameter allows the determination of increases of plastic strain for every step of analysis and to follow the process of strain accumulation. In the CDP model, these parameters was described as follows:

$$\tilde{\varepsilon}_t^{pl} = \tilde{\varepsilon}_t^{ck} - \frac{d_t}{(1-d_t)} \cdot \frac{\sigma_t}{E_0} \quad (3.1)$$

$$\tilde{\varepsilon}_t^{ck} = \varepsilon_t - \varepsilon_{0t}^{el} \quad (3.2)$$

$$\varepsilon_{0t}^{el} = \frac{\sigma_t}{E_0} \quad (3.3)$$

$$\tilde{\varepsilon}_c^{pl} = \tilde{\varepsilon}_c^{in} - \frac{d_c}{(1-d_c)} \cdot \frac{\sigma_c}{E_0} \quad (3.4)$$

$$\tilde{\varepsilon}_c^{in} = \varepsilon_c - \varepsilon_{0c}^{el} \quad (3.5)$$

$$\varepsilon_{0c}^{el} = \frac{\sigma_c}{E_0} \quad (3.6)$$

where:

- $\tilde{\varepsilon}_t^{ck}$, $\tilde{\varepsilon}_c^{in}$ – cracking strain, crushing (inelastic) strain,
- $\varepsilon_{t,c}$ – total strain (tensile, compressive),
- $\varepsilon_{0t,c}^{el}$ – elastic strain (tension, compression) in undamaged material,
- E_0 – initial stiffness.

The CDP model uses concepts of non-associated, multi-hardening plasticity. The illustration of the cracking strain used for the definition of tension stiffening data is shown in Fig. 6a. The illustration of the crushing strain used for the definition of compression hardening data is presented in Fig. 6b.

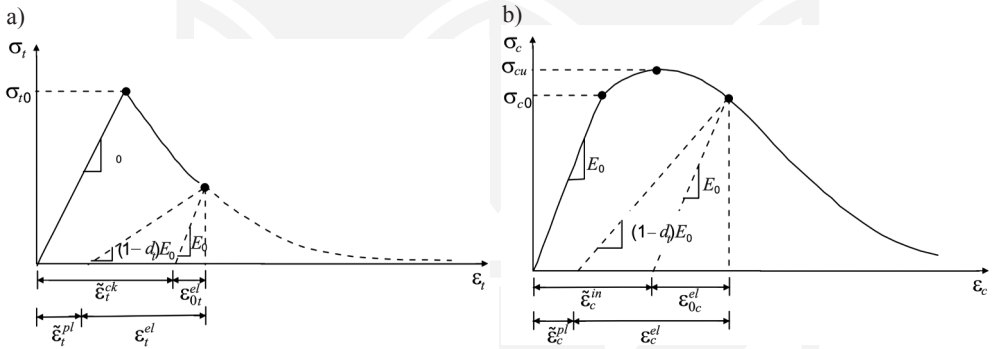


Fig. 6. Illustration of: (a) the cracking strain used for the definition of tension stiffening data, (b) the crushing strain used for the definition of compression hardening data [12]

Knowing the way in which damage parameters were determined, the parameter of the total stiffness degradation can be presented. The degree of stiffness degradation for elements depends on the relative occurrence of damage to tension and compression. This relation can be expressed by equation (4):

$$(1-d) = (1-d_c)(1-d_t) \quad (4)$$

Tensile damage variable d_t and compressive damage variable d_c can take values from zero (undamaged material) to one (total loss of strength).

The degradation process can be described by equation (5):

$$\sigma = (1-d) \cdot D_{0el} : (\varepsilon - \varepsilon_{pl}) \quad (5)$$

where:

- σ – stress matrix,
- d – stiffness degradation parameter,
- D_{0el} – elastic stiffness matrix,

ε – strain matrix,
 ε^{pl} – plastic strain.

The values of d_t and d_c parameters can be obtained experimentally. In this article, the value of parameter d was adopted from paper [7].

The values of the material parameters for B50 concrete are presented in Table 1. Other parameters of the concrete material were adopted as follows: tensile strength – 2.7 MPa, compressive strength – 49 MPa, dilation angle 38° .

Table 1

Parameters of the concrete damage plasticity model for B50 concrete [7]

| Parameter | | Value | |
|-------------------|-----------|------------------------|-----------|
| Young modulus | | 37 GPa | |
| Poisson ratio | | 0.2 | |
| Density | | 2500 kg/m ³ | |
| Damage parameters | | | |
| Strain (tension) | d_t [-] | Strain (compression) | d_c [-] |
| 0 | 0 | 0 | 0 |
| 0.00016 | 0.406 | 0.000761 | 0 |
| 0.00028 | 0.696 | 0.00255 | 0.195 |
| 0.00068 | 0.920 | 0.00567 | 0.596 |
| 0.00108 | 0.980 | 0.0117 | 0.895 |

5. Data of the mainshock and the aftershock

In the dynamic analysis, a registered sequence of Aquilliano seismic shocks was used for the kinematic excitation of the bridge [13]. The sequence consisted of the mainshock and the aftershock. The shocks occurred on 30th March 2009 in Italy with an interval of two hours. The original range of acceleration was scaled by 1.4 in the case of the mainshock and by 15 in the case of the aftershock to obtain similar values of PGA for both shocks. The time history of accelerations in three directions (horizontal north-east, horizontal south-west, vertical) are shown in Fig. 7–8.

It can be observed that the maximal value of acceleration in the NE direction for the mainshock was 1.97 m/s², whereas for the SW direction – 1.24 m/s². For the aftershock, these values equalled: 2.01 m/s² for the NE direction and the 1.77 m/s² for the SW direction. Values of horizontal PGA for both shocks were very close – 2.33 m/s² and 2.67 m/s² for the mainshock and aftershock, respectively. This case of seismic sequence differs from the typical sequence of shocks. In the vast majority of registered sequences, the mainshock is stronger than the aftershock. However, examples of sequences when the main shock is lower than (or equal to) the aftershock can be found from seismic databases (e.g. Itaca.net, PEER) [13, 14].

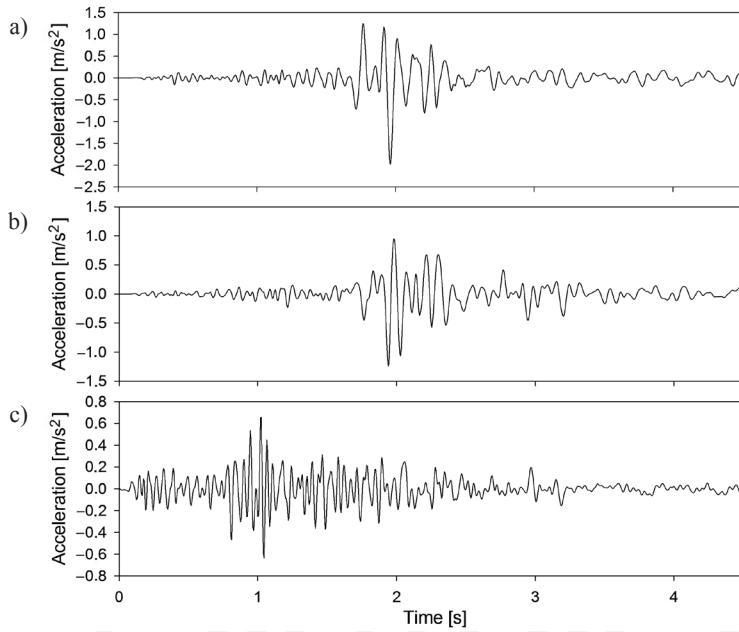


Fig. 7. Time history of accelerations of the mainshock in direction: (a) horizontal NE, (b) horizontal SW, (c) vertical Z

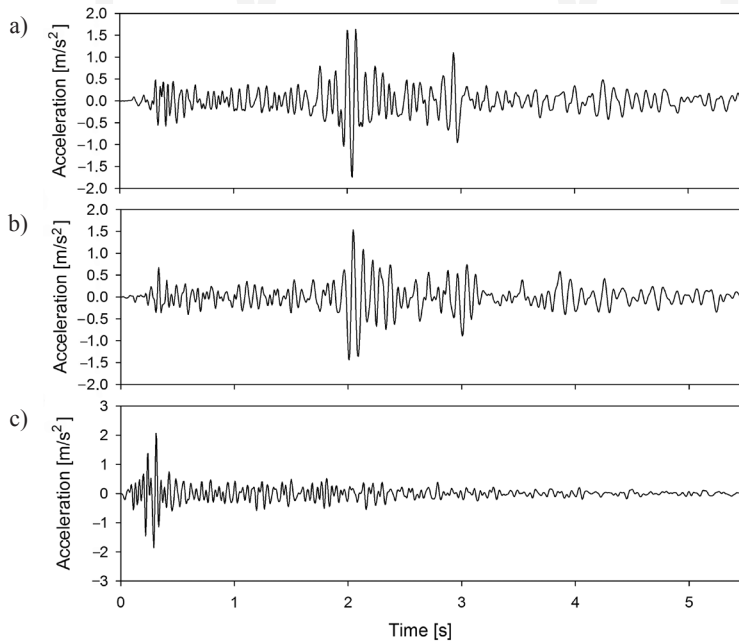


Fig. 8. Time history of accelerations of the aftershock in direction: (a) horizontal NE, (b) horizontal SW, (c) vertical Z

6. Dynamic analysis of the bridge under the sequence of seismic shocks

The dynamic responses of the bridge to both shocks were calculated using full-time history analysis. This was carried out with the Hilber-Hughes-Taylor time integration algorithm provided by the ABAQUS software. As the damage and failure model of concrete implements strong material nonlinearity, a step of numerical integration was not fixed. The step varied from 10^{-6} to 10^{-2} s, according to convergence requirements. The geometric nonlinearity was also taken into account.

The selected shocks were attached to the supports of the bridge as ground motions in three directions. In the longitudinal direction, the NE component was implemented; in the transverse direction, the SW component was applied.

For the dynamic analysis, the Rayleigh model of mass and stiffness proportional damping was applied. The damping coefficients $\alpha = 0.56$ (referring to mass proportional damping) and $\beta = 0.0013$ (referring to stiffness proportional damping) were determined for damping ratios of 5% for the first (5.36 Hz) and second (6.70 Hz) natural frequency.

The seismic performance of the bridge under the sequence of the mainshock and the aftershock was investigated in two steps. In the first step, the mainshock was applied to the structure; this resulted in the occurrence of some plastic and damage to areas of the bridge. The aftershock was then imposed on the bridge structure which had already been weakened by the first shock. The observed evolution of plastic and damage measures, incorporated into the concrete damage plasticity model of the material, allowed the assessment of the impact of both shocks on the bridge.

The basic variable that describes the concrete material performance during the shocks is the tensile damage parameter that shows the concrete material degradation in tension.

The bottom view of the beams of the outer bridge span after the entire sequence of shocks is shown in Fig. 9. It can be observed that the damage of structure occurred mainly in the middle of the bottom side of the outer span.

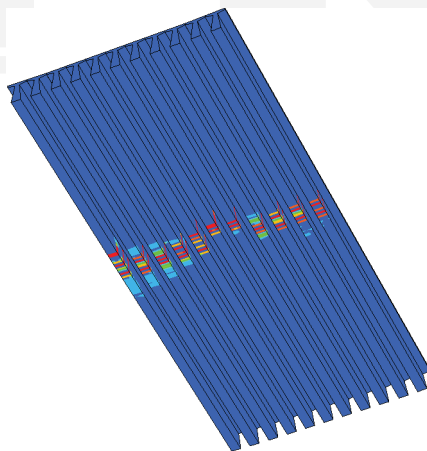


Fig. 9. The damaged area (coloured) in the middle of the outer span – bottom view

Detailed maps of tensile damage distribution in the middle of the span after the first and the second shock are displayed in Fig. 10.

On the basis of these maps, the noticeable increase in the level of damage to the structure due to the secondary shock can be observed. The largest changes in the level of damage were located in the area indicated in Fig. 10. During the mainshock, the tensile damage variable takes non-zero values in the middle of all beams. During the aftershock, the progress of deterioration that began during first shock takes place. The appearance of new damaged zones of the structure can be easily identified.

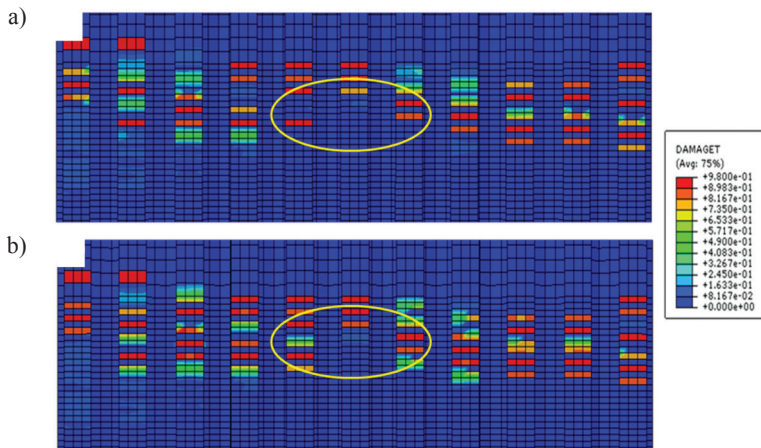


Fig. 10. Maps of tensile damage distribution in the middle of the span: (a) after the mainshock, (b) after the aftershock

To present the seismic performance of the bridge in terms of inelastic and damage behaviour of the concrete material under the sequence of the mainshock and the aftershock, a detailed time history analysis was carried out at numerous points of the superstructure. The results are shown at points P1, P2 and P3 located in the middle of the span (Fig. 11).

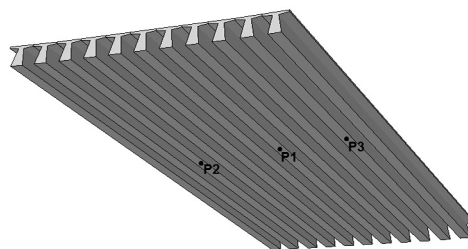


Fig. 11. Location of points selected to dynamic analysis

The following time histories of the plastic and damage measures at selected points were examined and are presented in Figs 12–14: logarithmic maximal and minimal principal

strain (LEP_{max} and LEP_{min}), equivalent plastic strain in tension (PEEQT), tensile damage parameter (DAMAGET). Logarithmic strain shows the dependence of total strain on time. For geometrically nonlinear analysis, logarithmic strain is the measure that takes into account the continuous variation of length. In the case of the concrete damage plasticity model, equivalent plastic strains in tension (PEEQT) and in compression (PEEQC) are separate measures of plastic behaviour under tension and compression. Hence, the equivalent plastic strain in tension is a parameter that controls the evolution of the cracking surface – this is linked to failure mechanism under tension loading. The tensile damage variable (DAMAGET) indicates damage occurring in the structure due to cracking. Finally, the stiffness degradation parameter (SDEG) indicates the loss of strength – it takes values from zero (representing undamaged material) to one (representing total loss of strength).

The time histories of plastic and damage measures at point P1, located in the central zone of the span, are shown in Fig. 12. When the amplitude of the ground oscillations enlarged substantially during the mainshock (2 sec) the concrete material went plastic (Fig. 12a) and failure of the concrete material (DAMAGET) occurred due to severe tension (Fig. 12b). The tensile damage at point P1 also contributed to the degradation of stiffness (SDEG). Until the onset of the first damage, the element stiffness had an initial value. The element damage triggered a sharp decrease of stiffness which was proportional to the tensile damage at the same moment (Fig. 12b).

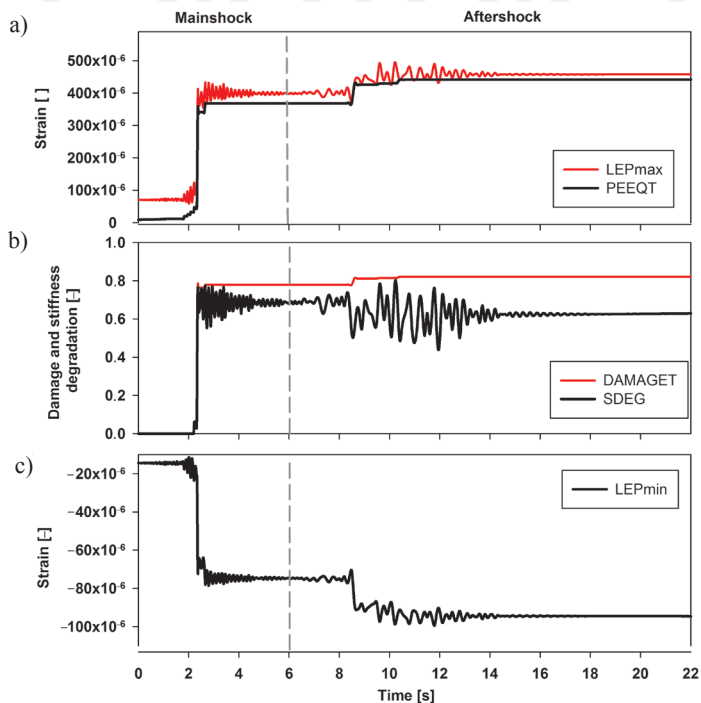


Fig. 12. Time histories at point P1 during the sequence of shocks: (a) logarithmic maximal principal strain (LEP_{max}) and equivalent plastic strain in tension (PEEQT); (b) tensile damage (DAMAGET) and stiffness degradation (SDEG) parameters; (c) logarithmic minimal principal strain (LEP_{min})

During the aftershock, only a small increase in principal stresses (both maximal and minimal) as well as in damage and stiffness degradation parameters were noticed. It is worth noting that the increase in the absolute value of minimal strain and the oscillations of this measure during the aftershock (2.4 sec) caused a slight recovery of the average element stiffness as well as the oscillation of this degradation measure (Fig. 12b). This phenomenon occurred due to the increase of compressive strain that partially closed cracks. After the mainshock, the average stiffness reduction reached 70% at point P1 whereas at the end of the aftershock, it was at a level of 60%.

On the basis of Fig. 12, it can be easily observed that the element damage occurred mostly during the first shock. The aftershock (with PGA comparable to the mainshock PGA) resulted only in a slight increase in the damage level. At the end of the mainshock, damage at point P1 was at a level of 80%, whereas after the secondary shock, it increased only by about 2–3%.

A different scenario, as far as the impact of both shocks is concerned, occurred at point P2 (Fig. 13). Contrary to the results obtained at point P1, only slight damage (1–2%) was recognised at point P2 during the mainshock. In actuality, this element was damaged during the secondary shock. Within 2.4 seconds of the aftershock, a significant leap of tensile damage (DAMAGET) appeared at point P2 (Fig. 13b). At the end of the aftershock, tensile damage of the element reached 80%.

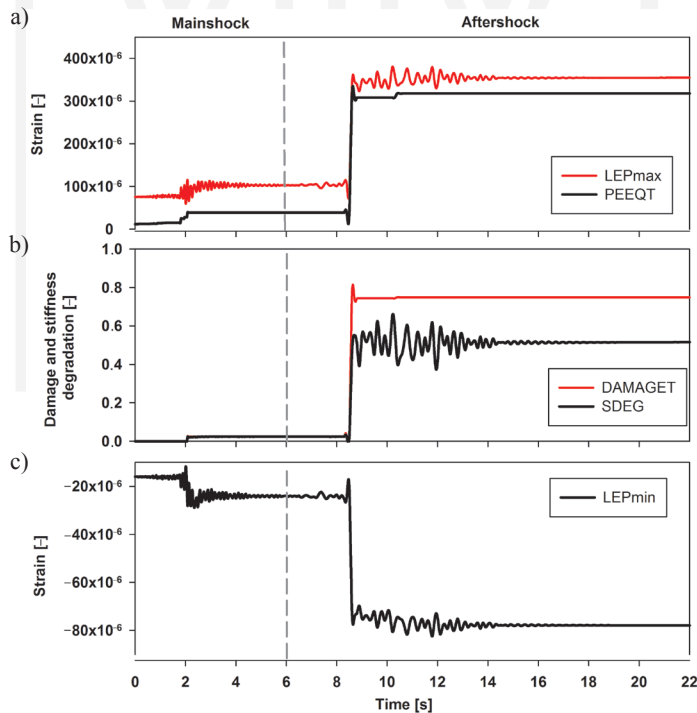


Fig. 13. Time histories at point P2 during the sequence of shocks: (a) logarithmic maximal principal strain (LEP_{max}) and equivalent plastic strain in tension (PEEQT); (b) tensile damage (DAMAGET) and stiffness degradation (SDEG) parameters; (c) logarithmic minimal principal strain (LEP_{min})

The rapid increase of plastic strain and tensile damage parameter were accompanied by the violent stiffness degradation at point P2. After 2.4 seconds of the aftershock, the oscillations of compressive strain produced the oscillations of stiffness. Finally, at the end of the aftershock, the stiffness degradation at point P2 reached 50%.

Finally, the dynamic performance of the concrete beam at point P3 was analysed. Diagrams presenting the time histories of plastic and failure parameters at point P3 during the sequence of shocks are shown in Fig. 14.

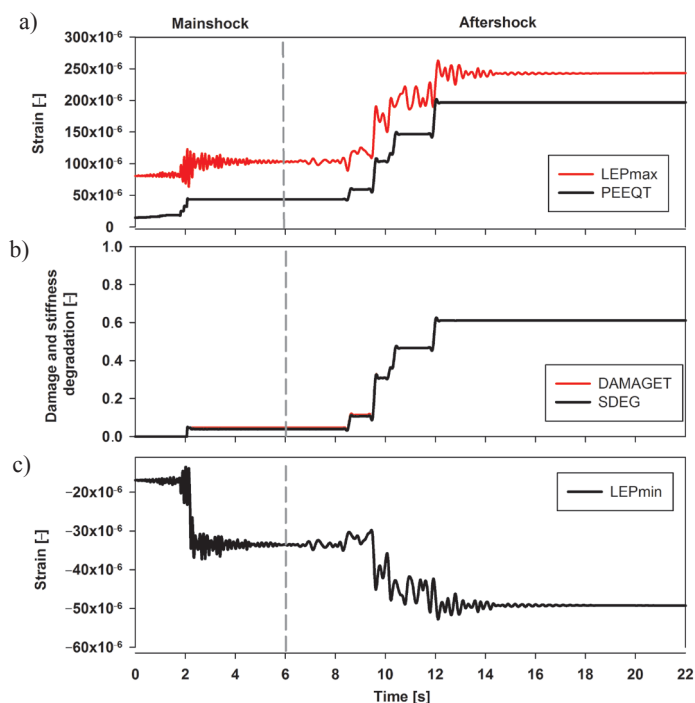


Fig. 14. Time histories at point P3 during the sequence of shocks: (a) logarithmic maximal principal strain (LEP_{max}) and equivalent plastic strain in tension (PEEQT); (b) tensile damage ($DAMAGET$) and stiffness degradation (SDEG) parameters; (c) logarithmic minimal principal strain (LEP_{min})

It can be noticed on the basis of Fig. 14 that damage to the element P3 appeared during both shocks. All diagrams clearly show consecutive stages of the increase in plastic and damage measures at point P3. They revealed that the first noticeable increase in principal strains, both compressive and tensile, occurred during the mainshock (Fig. 14b); however, the stiffness parameter indicated only a slight stiffness reduction (5%).

The progressive significant destruction at point P3 can be observed during the aftershock. Contrary to the previously examined points, P1 and P2, the stiffness degradation at point P3 did not appear rapidly but proceeded in time. Finally, the level of damage and stiffness reduction reached 65%.

The phenomenon of progressive damage is clearly visible in Fig. 14b. A strong correlation between the values of strain and the degree of the element damage could be observed. Because the element strain increased gradually, the tensile damage measure (DAMAGET) and the stiffness degradation parameter (SDEG) also enlarged gradually in relatively small leaps. An oscillation of the stiffness value was not observed. Despite the increase of minimal strain level, stiffness did not recover; this suggests that the element P3 was located in the tensioned zone where ‘closing up’ cracks did not appear.

7. Conclusion

The analysis of the dynamic performance of the reinforced concrete bridge subjected to the sequence of seismic shocks using the CDP material model allowed the formulation of the following conclusions:

1. Both the mainshock and the aftershock strongly affected the analysed bridge. The plastic behaviour and damage of the concrete material appeared in the bottom part of the outer span of the bridge. The increase in the element damage was accompanied by stiffness degradation which decreased proportionally to the degree of damage. The level of stiffness reduction reached 80% in the analysed zone.
2. Several scenarios of structure degradation can be distinguished under the sequence of the mainshock and aftershock with similar values of PGA. The damage and failure of some elements may occur during the mainshock only with the aftershock not increasing the degradation of the structure. However, the situation may be the opposite of this – the mainshock may not impose any damage to the structure, its degradation may be due to the aftershock only. Finally, the damage and failure process may propagate throughout the entire sequence of shocks.
3. The analysis revealed that the reduced element stiffness may be partially regenerated. This phenomenon occurs in elements where significant increase of compressive strain is observed and ‘closing up’ cracks appear.

References

- [1] Abdelnaby A., *Response of reinforced concrete structures under multiple earthquakes*, [PhD thesis], Urbana (IL), University of Illinois at Urbana-Champaign, 2012.
- [2] Abdelnaby A., Elnashai, A., *Response of degrading RC frames under replicate motions*, Proc. of the 15th World Conference on Earthquake Engineering (15WCEE), Lisbon 2012.
- [3] Dulinska J.M., Jasinska D., *Performance of steel pipeline with concrete coating (modeled with concrete damage plasticity) under seismic wave passage*, Applied Mechanics and Materials 459, 2014, 608–613.
- [4] Dulinska J.M., Szczerba R., *Assessment of concrete bridge performance under moderate seismic shock using concrete damage plasticity model*, Procedia Engineering 57, 2013, 1319–1328.

- [5] Fakharifar M., Chen G., Sneed L., Dalvand A., *Seismic performance of post-mainshock FRP/steel repaired RC bridge columns subjected to aftershocks*, Composites Part B: Engineering 72, 2015, 183–198.
- [6] Huang W., Qian J., Fu Q., *Damage assessment of RC frame structures under mainshock-aftershock seismic sequences*, Proc. of the 15th World Conference on Earthquake Engineering (15WCEE), Portugal, Lisbon 2012.
- [7] Jankowiak T., Łodygowski T., *Identification of parameters of concrete damage plasticity constitutive model*, Foundations of Civil and Environmental Engineering 6, 2005.
- [8] Kmiecik P., Kamiński M., *Modeling of reinforced concrete structures and composite structures with concrete strength degradation taken into consideration*, Archives of Civil and Mechanical Engineering XI (3), 2011, 623–636.
- [9] Lee J., Fenves, G.L., *Plastic-damage model for cyclic loading of concrete structures*, Journal of Engineering Mechanics 124(8), 1998, 892–900.
- [10] Lubliner J., Oliver S., Onate E., *A plastic-damage model for concrete*, International Journal of Solid and Structures 25 (3), 1989, 229–326.
- [11] Zhai, Ch-H., Zheng, Z., Li, S., Xie L-L., *Seismic analyses of a RCC building under mainshock–aftershock seismic sequences*, Soil Dynamics and Earthquake Engineering 74(7), 2015, 46–55.
- [12] Abaqus 6.14 Analysis User's Manual.
- [13] itaca.mi.ingv.it (access:10.11.2015).
- [14] peer.berkley.edu (access:10.11.2015).

